Review

Israel Journal of Chemistry

doi.org/10.1002/ijch.202100067

Bulk and Surface-Mediated Polymorphs of Bio-Inspired Dyes Organic Semiconductors: The Role of Lattice Phonons in their Investigation

Tommaso Salzillo,[a] Andrea Giunchi,[b] Lorenzo Pandolfi,[b] Aldo Brillante,[b] and Elisabetta Venuti*[b]

Abstract: Raman spectroscopy of organic molecular materials in the low-wavenumber region gives access to lattice vibrational modes and to the wealth of information on solid state properties that these can provide. In the field of organic electronics a useful application concerns the discrimination of the crystalline forms i.e. polymorphism of the semiconductor. The capability of characterizing and identifying the polymorphs of a compound is in fact the prerequisite for an exhaustive study of the charge transport characteristics which arise from the relationship between molecular, electronic, and crystal structures. Thus, the need is felt of a non-invasive, non-destructive tool such as Raman, which probes the crystal phase by detecting the lattice modes which are sensitive even to subtle variations of the packing. Here we review the contribution of the technique to the study of organic pigments displaying promising semiconducting properties and characterized by polymorphism both in their bulk and thin film phases.

Keywords: natural dyes · polymorphism · Raman spectroscopy · lattice phonons · organic semiconductors

1. Introduction

Organic molecular systems represent a widespread class of multifunctional materials with a variety of properties which can be exploited in several fields of application, from pharmaceutical to electronic industries. Following the early discovery of the semiconducting properties of anthracene and violanthrone,[1,2] research has developed in the field of organic electronics, aimed at finding valid substitutes for silicon electronic components, which are affected by high processability costs. Their low price in the raw state, combined with the versatility of the processing methods, have in fact transformed the organic materials from purely scientific curiosities to subjects of high technological interest, enabling the manufacture of completely new products.[3,4] Radio Frequency Identification (RFID) labels, flexible displays, solar cells, organic light emitting diode (OLED) for lighting and displays are just some of the innovative products based on organic semiconductors.[5] However, while OLEDs lead the market,[6] organic field effect transistors (OFETs) still lag behind, missing the features needed to replace silicon-based systems and displaying poor performances overall. Despite this, OFETs are still appealing for application niches not filled by conventional electronic technologies such as selective detection of chemical compounds or sensing platforms in bioelectronics.[7]

Recently, vat dyes of natural origin used traditionally for textiles, such as indigo and its derivatives, were shown to behave as semiconducting active materials in organic based OFETs.[8,9] The structural similarity to biological compounds and their potential bio-compatibility and non-toxicity,[10–12] suggest the use of both natural and nature-inspired dyes in biomedical applications.[13,14]

As with all molecular materials, the physical and chemical properties of the dyes are strictly correlated to the solid-state packing modes, which are governed by weak intermolecular force fields that comprise non-directional van der Waals forces, π-π stacking and hydrogen bonding.[15] The low strength of these interactions is primarily responsible for the occurrence of the well-known and central phenomenon of crystal polymorphism,[16] that in the organic compounds manifests itself via multiple structures of very close energies, often co-existing outside the range of their thermodynamical stability. On one hand, polymorphism is a source of physical impurity which impairs reproducibility in the charge transport properties of the system and must be prevented. On the other hand, it represents an additional degree of freedom in the design of the semiconductor, as it allows it to be tuned for optimal packing.[17] What is certainly true is that polymorphism is experimentally difficult to predict, control and

[a] *T. Salzillo*
Department of Chemical and Biological Physics,
Weizmann Institute of Science,
Herzl Street 234, 76100 Rehovot, Israel
[b] *A. Giunchi, L. Pandolfi, A. Brillante, E. Venuti*
Dipartimento di Chimica Industriale "Toso Montanari", and
INSTM-UdR Bologna,
Università di Bologna,
Viale del Risorgimento 4, Bologna, 40136 Italy
E-mail: Elisabetta.venuti@unibo.it

rationalize, as it depends on a great deal of not easily controllable variables. The most effective way to deal with it is to apply multiple techniques to its detection and investigation, possibly complementary and alternative to the technique of choice for the study of the crystal structure, that is X-ray diffraction.

In the last decade, low-wavenumber Raman microscopy has proven to be a versatile, reliable and fast way for the identification and the spatial mapping of crystalline phases in molecular material-based devices.[18,19] Different structures can in fact be identified on the basis of their spectrum in the THz region, which represents the fingerprint of the crystal lattice dynamics.[20] The modes observed here hold the character of lattice phonons, or vibrations in which molecules oscillate as a whole around the lattice equilibrium positions, subjected to the intermolecular force field. Weak restoring forces, combined with the high inertia momenta of the molecular body, determine the mode low energy, while the spectral features depend on the details of the interaction pattern brought about by the crystal packing. As each polymorph thus displays its own unique spectrum,[20–22] the Raman spectrum recorded in this range becomes an optimal probe of the structure itself.

This review summarizes the work of our group in the investigation conducted by lattice phonon Raman microscopy on the polymorphism of a series of dyes that have proved interesting in the manufacture of OFETs (Scheme 1).[9,23–25] Such a work has benefited from the precious support of highly accurate DFT calculations including a-posteriori dispersion (or van der Waals, vdW) corrections (DFT-vdW).[26–28] This was done both to assess the relativity thermodynamical stability of the polymorphs and to assist the spectroscopic investigation with finally reliable estimates from first principles calculations

Tommaso Salzillo graduated in Industrial Chemistry in 2011 and he received his Ph.D. degree in physical chemistry in 2015 from the University of Bologna. Currently he is holding a position as a Senior Postdoc at Weizmann Institute of Science working on the structural dynamics of functional materials by means of low-wavenumber Raman spectroscopy. Previously he was awarded with a Marie Curie Postdoctoral Fellowship at Institut de Ciència de Materials de Barcelona (ICMAB-CSIC) where his research project focused on the study of polymorphism and morphology control in flexible organic electronic devices. His research interests include polymorphism in organic semiconductors and active pharmaceutical ingredients, solid-state reactions and vibrational spectroscopy.

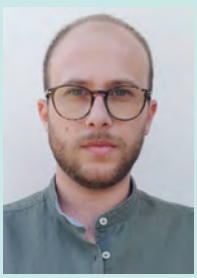

Andrea Giunchi is currently a research fellow at the University of Bologna. He completed his bachelor's (2015), master's (2017) and Ph.D. (2021) degrees in Industrial Chemistry at University of Bologna. His research interests lie in pharmaceutics and organic electronics with the aim of simulating energetic, structural and vibrational properties of the condensed matter by means of periodic DFT calculations based on plane waves. In particular, he has worked to the exploitation of the synergy between experiments and calculations in the polymorph screening of molecular crystals using vibrational techniques.

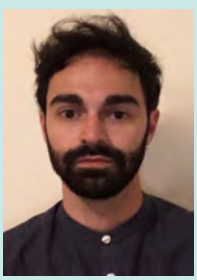

Lorenzo Pandolfi is currently a Ph.D. student in Chemistry at the University of Bologna. He obtained his bachelor's (2017) and master's (2019) degrees in Industrial Chemistry at the same University. At present, he works on solid-state characterization of organic semiconductors, polymorph screening of active pharmaceutical ingredients (APIs) and crystal-to-crystal photoreactions by means of lattice phonon Raman microscopy, X-ray diffraction techniques, infrared and UV-Vis spectroscopies with the synergic support of DFT calculations.

Aldo Brillante is a retired professor of Physical Chemistry of the University of Bologna. Graduated at the University of Bologna and former postgraduate student of D.P. Craig (Australian National University), he was appointed in the mid seventies by IBM Research Laboratories (San Jose) as postdoctoral Fellow in a surface science project. In the following years he spent several periods at the University of Düsseldorf (surface plasmons) and at the MPI FkF Stuttgart (high pressure spectroscopy). His activity has been mostly dedicated to the study of elementary excitations in solids (excitons, phonons, plasmons and polaritons). He is currently studying polymorphism, crystal-to-crystal photoreactions and lattice phonons.

Elisabetta Venuti is Associate Professor in Physical Chemistry at the University of Bologna. A former student at the University of Florence and at CNR (Bologna), she was a postdoctoral researcher at the Max-Planck Institute in Mülheim a.d. Ruhr (DE) and visiting scientist at the Universities of Reading (UK) and Helsinki (FI). Her research has dealt with the experimental and computational spectroscopic response of molecular systems in the gas and condensed phases by means of high resolution IR, time resolved fluorescence and solid state Raman techniques. Recent activity has focused on the study of structural and dynamics properties of materials for organic electronics.

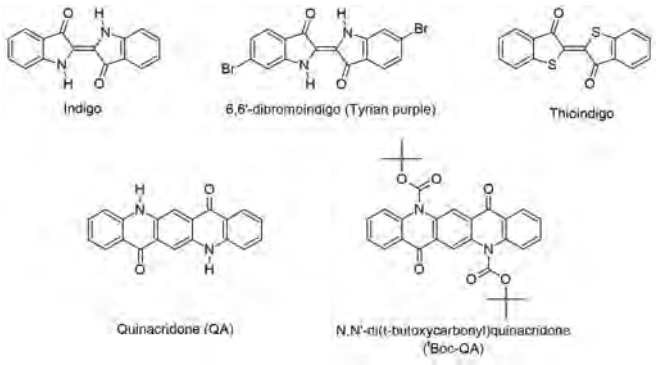

Scheme 1. Molecular structures of the organic dyes and its latent precursor reported in this work.

of energies and intensities of intermolecular vibrations. The focus of this work is necessarily on experiments, but how these can be reliant on theoretical predictions is fully described in ref. [28] and will emerge clearly throughout our report.

The layout of the work is the following. Section 2 is dedicated to the experimental setups that can be used to reach the low-frequency range; Section 3 deals with examples of polymorphism of the systems under study in the bulk phase, showing how this knowledge assists in the understanding of the occurrence of surface-mediated structures; finally in Section 4 the spectroscopic approach is applied to the characterization of thin films grown by high-vacuum evaporation or by different solution approaches.

2. Low-Wavenumber Raman: Experimental Setup

Low-wavenumber Raman spectroscopy, also called Raman spectroscopy in the THz range, is in this context a conventional Raman technique in which the scattering signal can be collected over an energy range that is very close, ideally by only a few wavenumbers, to the intense line of the elastic Rayleigh scattering. The lower limit of the detection is, of course, determined by the characteristics of the measurement apparatus. The spectral window involved is instead not univocally defined, as it depends on the nature of the systems itself. In molecular solids, the boundary between high and low wavenumber ranges is determined by the transition from those classified as inter- (low energy) and intra-molecular (high energy) vibrational modes. Thus, for inorganic systems, the window of interest is wide and can reach and even overcome 600 cm^{-1},[29] while for organics the range can be usually restricted to 150 cm^{-1}.[22,27,30–33] A phenomenological approach suggests selecting the range where only those modes that do not belong to the spectrum of the isolated molecule appear. However, although very useful, the idea of a complete separation between inter- and intra- molecular degrees of freedom is sometimes notional, as it depends on molecular characteristics such as flexibility and each case must be individually considered.[20]

To eliminate the Rayleigh component, the most common Raman spectrometers available on the market use holographic notch filters, that can however barely record the low-wavenumber spectral region, because of their considerable bandwidths, typically >200 cm^{-1}.[34] With such a value, both the Rayleigh scattering and a large portion of the low-wavenumber range of interest are cut out. Satisfactory low-wavenumber detection limits can be achieved by means of three different experimental strategies: filters based on the absorption lines of an atomic or molecular vapor; triple-stage monochromators or, more recently, volume Bragg gratings as ultra-narrow optical filters, also known as Ultra-Low frequency Filters (ULF).

The first approach is quite uncommon, due to the complexity of the experimental setup and the data treatment. The Rayleigh line is absorbed by a gas of atoms or molecules heated at a specific temperature. A recent work described the use of molecular iodine gas filters for the absorption of the very narrow laser lines of an Argon ion laser. Indeed, iodine vapor presents a very narrow (1 GHz) vibronic absorption line close to the laser 514.5 nm emission, and its elimination efficiency turns out to be of the order of 10^6.[35] The most recent and widespread strategy is the use of the volume Bragg gratings (VBG) as optical filters for the Rayleigh scattering rejection. A VBG is a diffractive grating produced by refractive index modulation in the volume of a photosensitive material (normally photo-thermo-refractive (PTR) glass is employed).[34] VBG filters have diffraction efficiencies as high as 99.99% with a linewidth narrower than 1 cm^{-1} at FWHM, 5–10 cm^{-1} cut-off frequency and Rayleigh light rejection with optical density OD = 1-4. An optimal signal to Rayleigh scattering ratio is usually higher, so for the best data collection VBG filters need to be used in series, as schematically shown in Figure 1a (ULF_1, ULF_2), reaching the elastic scattering suppression by at least six orders of magnitude. Employing VBGs gives access to the low-frequency range simultaneously for the Stokes and anti-Stokes with a good rejection of the Rayleigh light in an easy experimental setup.[30,36,37] Among possible disadvantages is the necessity of a set of VBG filters for each specific wavelength, unless multiplexed filters are used, and the loss of a linear response for the Stokes and anti-Stokes, especially for the high frequency regions.[34]

A well consolidated experimental approach, which is nowadays considered outdated, employs triple grating spectrometers (Figure 1b) working in double subtractive and single additive configuration. This allows access to the low-frequency range with a cut-off of 4 cm^{-1}, but the simultaneous collection of Stokes and Anti-Stokes regions is not practicable. The rejection of the Rayleigh scattering is due to the first two gratings, while the third one is responsible for the dispersion stage. The advantage of such a setup consists in its versatility, as it can operate with any laser line with high spectral resolution, but unfortunately this is achieved at the expense of the apparatus brightness.

Israel Journal of Chemistry

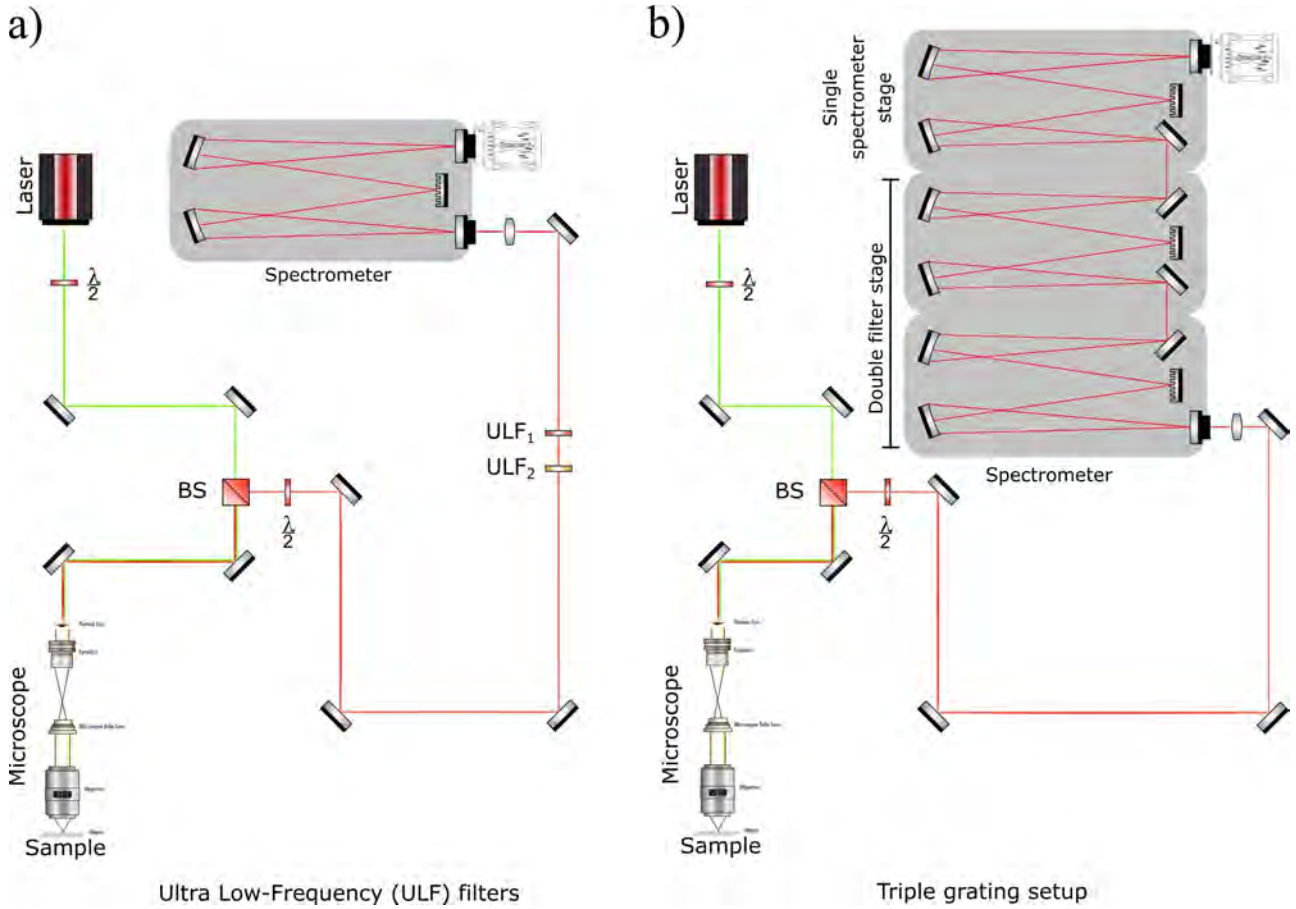

Figure 1. Schematic representation of the two experimental configurations which allow to access the low-wavenumber Raman energy interval. Set up employing ultra low-frequency (ULF) filters (a) and set up equipped with triple gratings operating in double subtractive + additive mode (b).

The low-wavenumber micro-Raman spectra reported in the present review were obtained with a Horiba-Jobin Yvon T64000 triple grating Raman spectrometer, operating in double subtractive mode and interfaced with an optical microscope (Olympus BX40) with 10×, 20×, 50× or 100× objectives. Working in confocal mode allowed us to achieve a spatial resolution below 0.9 μm with the 647.1 nm excitation line. For most systems, the spectra were recorded spanning the low-wavenumber region of the lattice phonons ($< 150\ cm^{-1}$), and up to about 2000 cm^{-1} to detect the intramolecular vibrations. The excitation was from an Argon or Krypton ion lasers tuned at the lines 488, 514.5, 647.1, 676.4 and 752.5 nm, depending on the optical absorption properties of the specific sample. When required by the experimental conditions, the impinging laser power was attenuated with a series of neutral density filters to prevent crystal damage, a common occurrence for organic compounds, and care was taken to keep the actual power focused on the sample to less than 1 mW.

3. Polymorphism in Natural and Nature-Inspired Dyes

Polymorphism is a common phenomenon,[38] and, as noted above, can be considered an additional degree of freedom of the molecular material, facilitating the modulation of the properties in the condensed phase.[17]

Depending on the nature of the system it is possible to distinguish between packing or configurational and conformational polymorphs, following the definition made in 1965 by McCrone.[39,40] In the first case, different packing motifs occur for a single molecular geometry, either because of structural rigidity or of the presence of a very stable conformer.[27,41] Conformational polymorphism is instead typical of highly flexible molecules, which can pack in different structures exhibiting different molecular geometries or shapes.[40,42] In packing polymorphs, where the molecular configuration is the same due to the system rigidity, the low energy range of the vibrational spectrum usually carries all the spectral differences among distinct lattices. On the contrary, conformational polymorphs can be often easily distinguished over the range of

the intramolecular normal modes, as different spatial atomic arrangements in the molecule are associated with different vibrational frequencies.[43] Organic dyes are usually characterized by a rigid core and are therefore candidates for packing polymorphism. Overall rigidity in these systems is also enhanced by the strong H bonds which govern the molecular assemblies.[44] However, the weak intermolecular forces that accompany the strongly directional ones can modify, even slightly, the interaction energy with the functional groups involved in the H bonding also for small structural variations and in the presence of robust synthons. As a result, differences in the frequencies of modes connected with these groups are observed among polymorphs, as in the case of all indigoids. More importantly, the possibility of forming different synthons, starting from different pattern of interactions, still leads to different supramolecular arrangements which can be associated to the case of distinct conformers, with repercussions on the appearance of the vibrational intramolecular spectra, as for quinacridone.[45,46] Section 3.1 is dedicated to the study of the polymorphism of these systems in the bulk.

In organic electronics applications, the crystalline material is mostly used in the form of a thin film on a dielectric substrate. The contact with a solid surface influences the structural order, altering both the kinetics and the thermodynamics of the crystallization process. As a result, the stabilization of kinetic polymorphs may be induced, or even the formation of altogether new polymorphic modifications. These crystalline systems, that go under the name of surface induced polymorphs (SIP), surface mediated structures or thin film phases, depending on their nature and description, have been widely described and commented in the work by Jones et al.[47] Here we report the contribution of lattice phonon Raman spectroscopy to the understanding and description of such systems in Section 3.2.

3.1 Polymorphism in Bulk

We deal with two typical examples of bulk polymorphism in dyes for which the application of low-wavenumber Raman microscopy has increased the amount of information on the structures, elucidating processes of concomitant growth at micrometer scales and the possible occurrence of disorder. Both cases, indigo and quinacridone, are representative of systems in which hydrogen bonds play a preponderant role, which translates into two very similar polymorphs for the former and four quite different ones for the latter.

3.1.1 Indigo as an Exemplary Case of Concomitant Growth

Indigo [2,2'-bis(2,3-dihydro-3-oxoindolyliden)] is one of the most valued and globally widespread natural dyes, used in ancient and present times, even though its production has been virtually only industrial since its first synthesis by Alfred Bayer around 1880.[48] In addition to its exploited properties as a dye, in the past years indigo has attracted a renewed interest in materials science as a promising biocompatible semiconductor, which exhibits ambipolar transport in organic thin film transistors (OTFTs), with balanced hole and electron mobilities of $1 \times 10^{-2}\,cm^2\,V^{-1}\,s^{-1}$, and stability against degradation in air.[8,9,44] Indigo-based devices have been reported to have strong performance variability, depending on the experimental conditions used for the fabrication of the semiconducting active layer. Such a variability has been attributed to the occurrence of different polymorphic modifications,[49] but X-ray diffraction techniques cannot easily identify the phase present in films.[50] We have tackled the problem by adopting the strategy to study by Raman first the polymorphism in the indigo bulk, and then transfer this knowledge to the investigation of the films, as reported in Section 4.

Crystalline indigo is found with two polymorphs, named A and B.[51–55] Both are monoclinic $P2_1/n$ with 2 molecules per unit cell, sitting on inversion centres. In both polymorphs the full C_{2h} symmetry of the isolated molecule is virtually retained, and the molecular units interact in the crystal through a network of strong H-bonds, while forming parallel stacks of the aromatic cores via face-to-face π-π interactions. The two structures are therefore very similar, with A having the higher density at ambient conditions (about 3 %), and according to the density rule[56] this is the form predicted to be thermodynamically stable at absolute zero. This conclusion is confirmed by DFT-vdW simulations,[57] as at 0 K form A is computed to be more stable than B by 0.1–0.3 kcal/mol, depending on the method employed. Such a difference may appear small but is still in the range found by theoretical treatments for many packing polymorphs. The similarity between the structures and the energies might certainly explain why the phenomenon of concomitant growth[58] occurs for bulk indigo[57] and on such a small scale of the crystal size that the use of the micro-Raman technique (vide infra) has proved invaluable for identification.

The interpretation of the experimental Raman spectra of indigo in the low-wavenumber region takes advantage of the application of the so-called rigid body approximation for molecular crystals. Based on the assumption that intermolecular and intramolecular force fields are characterized by very different energies, the approximation allows the relative degrees of freedom to be treated separately, which corresponds to assume the molecules as rigid when the vibrational modes depending on the intermolecular potential are considered. DFT-vdW calculations of the normal modes confirmed the validity of the approximation for indigo, as the eigenvectors of the six Raman active modes of lowest energy (of symmetry $3A_g + 3B_g$) were found to describe rigid body translations and rotations, with no contribution of intramolecular terms.

Due to the low solubility of indigo in most solvents, crystal specimens for structure characterization must be obtained by vapor-based techniques. Single crystals were grown by Physical Vapor Transport (PVT) and by sublimation in nitrogen atmosphere. The crystals obtained by PVT (Figure 2a) were identified as being of form A by single-crystal X-ray diffraction (SCXRD) and were characterized by Raman

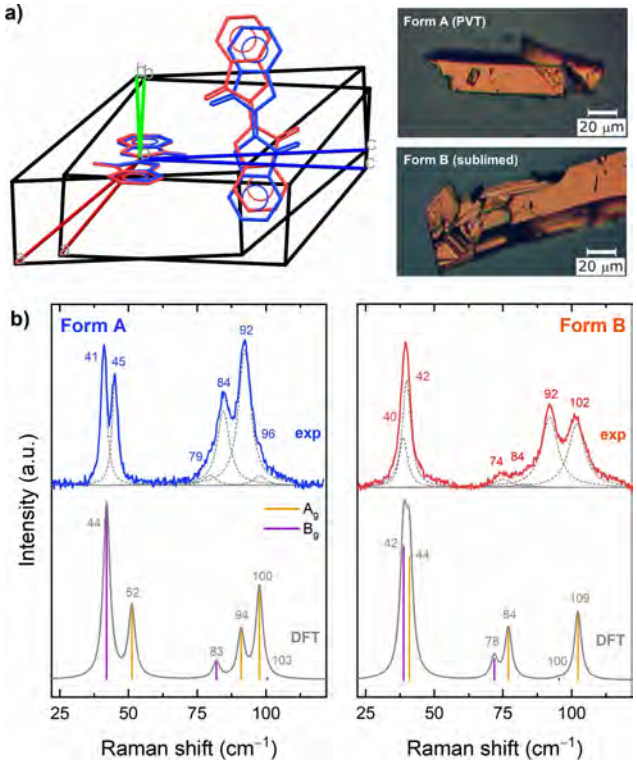

Figure 2. a) Left: overlay of the packing diagrams of indigo forms A (light blue) and B (orange), highlighting the small differences in the polymorphs unit cells and molecular orientations; right: images of their single crystals; b) DFT-vdW simulated and experimental Raman spectra of A and B indigo polymorphs in the lattice phonon energy range. The experimental spectra have been deconvoluted as sums of Lorentzian bands. Vertical bars of height proportional to the intensity of the mode identify the calculated values, with colour codes yellow and violet for modes of symmetry Ag and Bg, as indicated.

spectra in low-wavenumber range to get the unique lattice phonon Raman pattern for this polymorph. Both the sublimed and commercial materials did not contain sufficiently large single crystals and were analysed only by powder XRD.

The sublimed samples were found to be composed of both form A and B, with B prevailing, whereas the commercial material, unexpectedly, only of form B. In both cases crystallites of polymorph B could be singled out and measured by Raman microscopy, obtaining the lattice phonon spectrum of a single crystal. The labor of associating spectra to structures may appear a light one when described in a published work, but most often it is a tiresome trial-and-error procedure. For indigo, for instance, the samples to probe by XRD were chosen by recording *a-priori* Raman spectra on many crystallites, finally selecting those that displayed a range of different spectral features. In response to the XRD results, growth methods and conditions were modified and adjusted. For indigo, like in most of the cases presented in this work, the morphologies of the different forms were so alike that could not be used for the selection. Overall, it is often difficult to gain control over the crystallization process and selectively obtain a desired polymorph.

Lattice phonon Raman spectra of both polymorphs A and B, together with those obtained by DFT-vdW calculations, are shown in Figure 2b. Despite their structural similarity, the two forms can be easily distinguished by their spectral characteristics. Also, the experimental features which allow for their identification are well reproduced by the simulations.

In packing polymorphs molecular geometry does not change with the crystal structure and therefore intramolecular vibrational spectra are usually ineffective for polymorph screening. Indigo represents an exception to such a rule. Its strongest Raman band corresponds to a mode that comprises the bond stretching of the entire cross-conjugation chromophore.[59,60] This includes the central C=C and the acceptors C=O but embraces also the two N–H donor groups, as shown in Figure 3a, *i.e.* all the atoms that can be involved in intra- and inter-molecular H-bonds.

In the crystal, the band splits into a doublet (Figure 3a), which lies at 1578/1592 cm^{-1} and 1576/1587 cm^{-1}, for polymorph A and B, respectively. Such measurable differences in splitting and frequencies are a result of how even small modifications of the H-bond pattern affect the strength of the involved chemical bonds, impact on the vibrational dynamics of the system and are detected by Raman.

The ease with which a polymorph is obtained can be subjected to considerable variations over time, as a result of many often uncontrollable factors, and the literature reports numerous examples.[61,62] The indigo system does not escape this fate. Initially described as highly metastable compared to A, form B appears to grow as concomitant in most cases, and even becomes clearly predominant in commercial samples. By

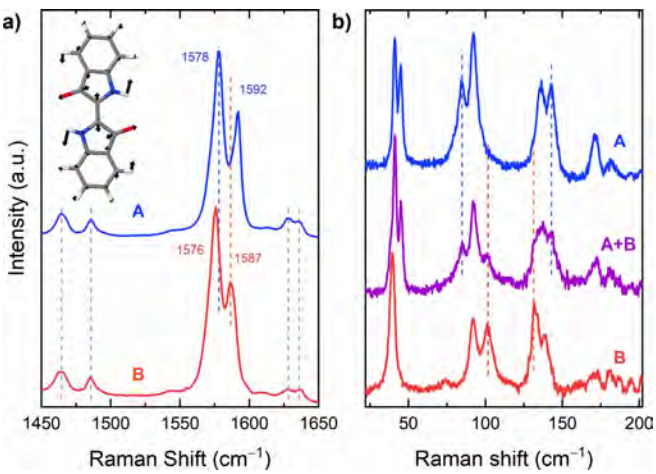

Figure 3. a) Raman spectra recording in polymorphs A and B the most intense and characteristic bands of indigo, corresponding to stretchings of the central C=C bond; b) the lattice phonon Raman spectra of an indigo microcrystal (purple trace) reveals the coexistence at a micrometric scale of both A and B polymorphs (blue and red traces are reference spectra of the pure A and B forms, respectively).

micro-Raman, the co-existence of the two indigo polymorphic modifications at a microscale level can be checked on a crystallite having the appearance of a single crystal but clearly showing at the lateral resolution ≈1 μm the lattice phonon bands of both for forms (Figure 3b), pinpointing a situation in which the two polymorphs co-exist as different micrometric domains in the same specimen.

With the situation of the indigo polymorphs clarified in the bulk, the Raman characterization can be extended to encompass thin films. Here the spectroscopic technique accomplishes the task of identifying B as the only form appearing on surfaces, even though the XRD discrimination is impaired by the likeness of the two structures.

3.1.2 Quinacridone's Many Polymorphs

Quinacridone (5,12-dihydroquinolino[2,3-b] acridine-7,14-dione, QA, Scheme 1), is a derivative of the natural origin compound acridone. Commercially known as Pigment Violet 19 (PV-19), QA is a dye widely used industrially for its low-cost and high stability.[24] Like for indigo, amine and keto groups are responsible for the extended hydrogen bond networks that characterize its condensed state. The good electronic properties which allow for its use as active material in field effect transistors[8] and photovoltaic devices[63] are attributed both to the hydrogen bonds and to π-π stacking interactions.

After years of debates and contradictory results, the situation regarding the many polymorths of QA was rationalized by Paulus at al.,[64] in a work based on a combined experimental and computational approach. Thanks to this accurate structural study, it is now accepted that pure QA can be obtained in four different forms, named α^{I}, α^{II}, β and γ (Figure 4a).[64,65] The two α forms can only be obtained as powders:[66] polymorph α^{I} has a triclinic $P\bar{1}$ structure with 1 molecule per cell; polymorph α^{II} is monoclinic, probably $P2_1/c$ with 2 molecules per cell. In both phases chains are formed by molecules bound *via* a pair of H-bonds to each of the two nearest neighboring molecules.[65] In turn, chains are arranged to form layers that lie all parallel to each other in α^{I}-QA and in a herringbone pattern in α^{II}-QA (see also Figure 5 of Ref. [65]) In fact, the two motifs can be randomly combined and it has been suggested[65] that the ideal α^{I}-QA and α^{II}-QA are just the

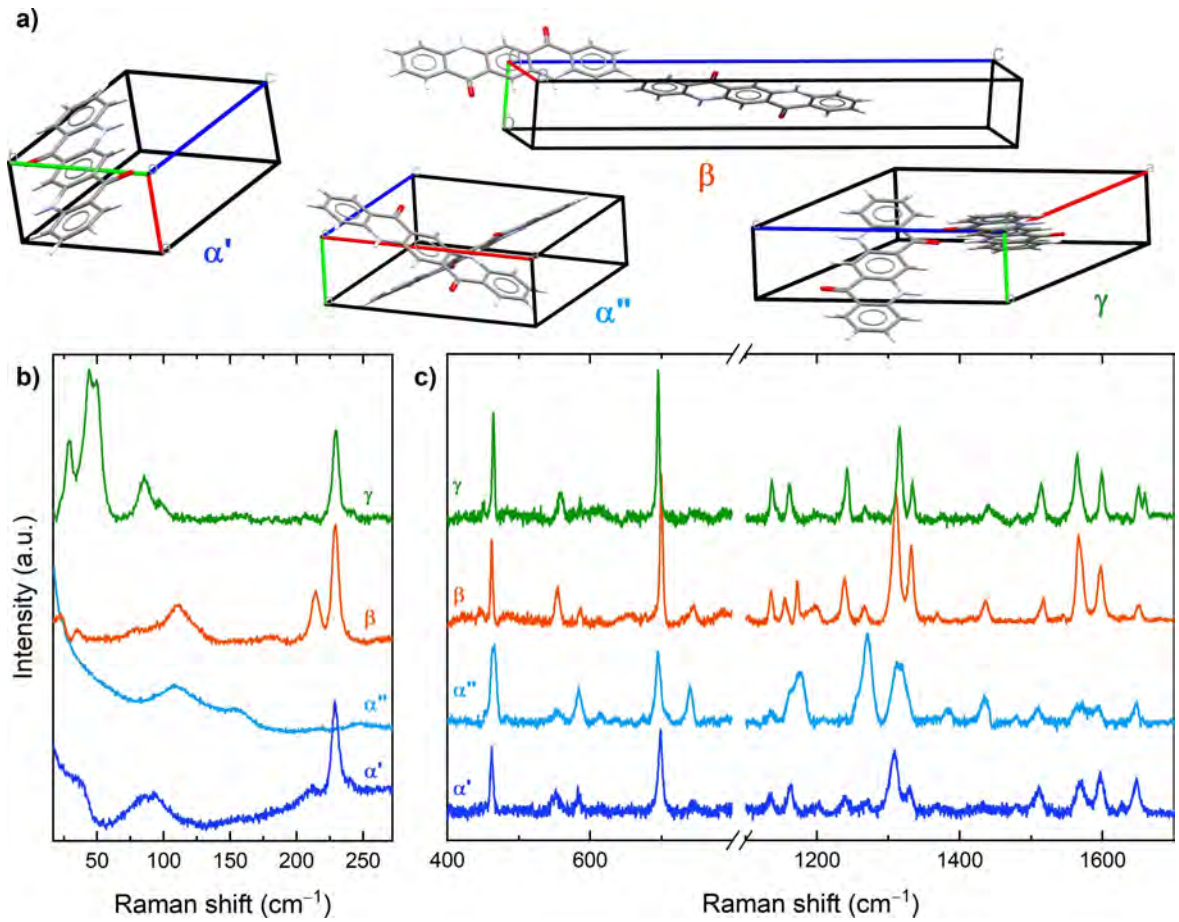

Figure 4. Raman spectra of α^{I}-, α^{II}-, β- and γ-QA powders in the low (a) and high-wavenumber (b) spectral regions. X-ray crystal structures for the four polymorphs are shown.

Israel Journal of Chemistry

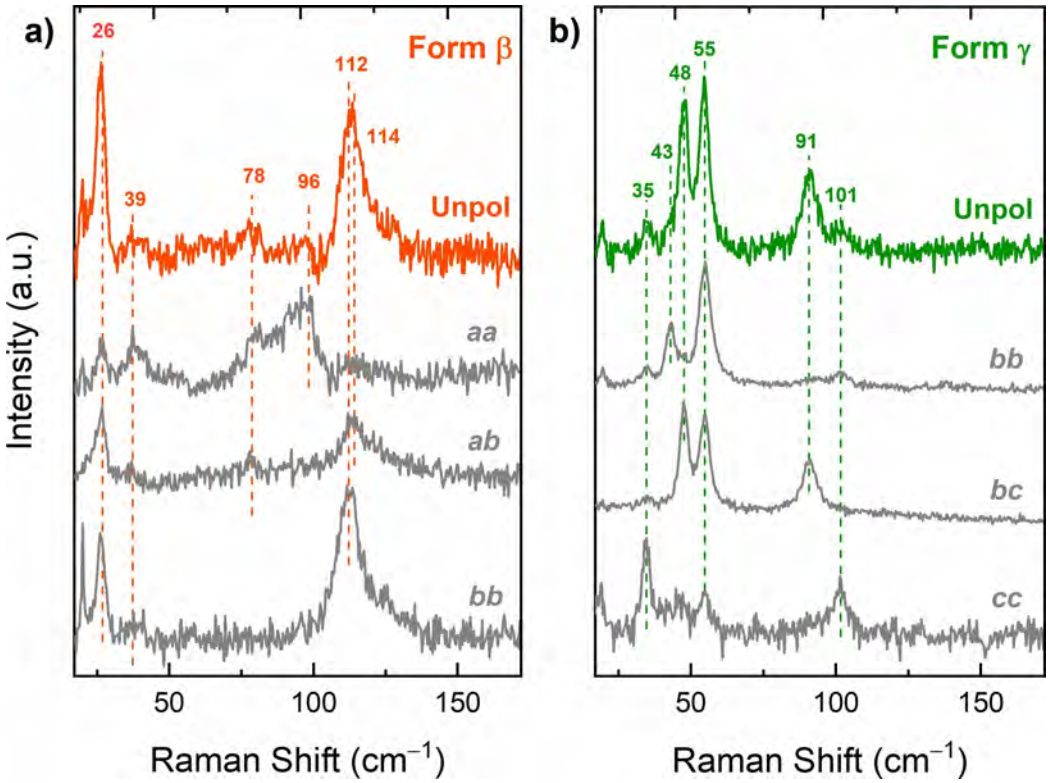

Figure 5. Polarized low-wavenumber Raman spectra of β (left panel) and γ (right panel) QA single crystals. Except for the Unpol spectra, the grey traces were recorded in crossed (B_g modes, *ab* and *bc*) and parallel polarizations (A_g modes, *aa*, *bb* and *cc*).

end structures of a series of disordered structures consisting of different percentages of each packing type, depending on the method and conditions used for their growth. Polymorphs β and γ can be grown as single crystals by PVT in closed and open systems, respectively. These structures, thermodynamically more stable, are both monoclinic $P2_1/c$ with 2 molecules/cell but contain very different H-bond arrangements.[65] In β-QA, the H-bond motifs are the same as in α structures, with the layers displaying two different chain orientations (see Figure 5 of Ref. [65]); in γ-QA, instead, each molecule is connected by single hydrogen bonds to four neighbouring molecules, so that the molecules are not arranged in chains, but form a criss-cross pattern. Low and high wavenumber Raman spectra for the four polymorphs are shown in Figure 4b,c, together with their structures.

Because of the stiffness of the QA molecule, the rigid body approximation can be adopted for the study of the low energy region. Following this, the observation of three and six Raman active phonon lattice modes is expected for α^{I}-QA and α^{II}-QA, respectively. One broad spectral feature is clearly identified around 97 cm^{-1} in α^{I}-QA, while two broad bands centred at 100 and 150 cm^{-1} appear for α^{II}-QA. Interestingly, the predicted disorder of the two phases reflects not only on the peak broadening but can also be confirmed by a specific low-wavenumber Raman signature. Indeed, when comparing the low-wavenumber region of all the four polymorphs in Figure 4b, it is evident that the two α phases display the so-called Rayleigh wing.[67]

The appearance of such a feature is an effect more common in inorganic materials, where it is called "central peak", and is an indication of some kind of disorder. For instance, a wide Rayleigh wing is characteristic of spectra of light scattered in liquids and is indicative of disorder-order phase transitions.[67]

In the framework of the rigid molecule approximation, six Raman active lattice vibrations are expected, (3 of A_g and 3 of B_g symmetry see Figure 4b) for both β-QA and γ-QA,[68] an assumption confirmed by a detailed study of the polarized Raman spectra (Figure 5) and DFT-vdW calculations.[45,69]

The spectral region of Figure 4b is extended to include the pair of bands that lie between 200 and 250 cm^{-1}. These correspond to modes that are mostly intramolecular in character, and are therefore expected to be almost dispersionless, with bandwidths[70] not affected by lattice disorder and defects, or by the dimension of the crystal domains. A band at 216 cm^{-1} is detected only in α^{I}-QA and in β-QA, albeit broader and weaker in the former, but is not present in γ-QA. The band of the intramolecular mode around 230 cm^{-1} lies at higher wavenumber in γ-QA with respect to α^{I} and β polymorphs. None of these features appear in α^{II}-QA, for which the first detected band is observed near 250 cm^{-1}, broad and very weak. Not surprisingly, the Raman spectra of α^{I}-QA

and β-QA look alike, due to the same hydrogen bond pattern in the two structures.

Figure 4c shows the powder Raman spectra α^{II}-, α^{I}-, β- and γ-QA polymorphs in the high wavenumber range. As already noted, the crystal structures of all the polymorphs are characterized by different networks of strong H-bond interactions. In this case, even if the QA molecule can be assumed to be rigid and only packing polymorphs are identified, the H-bond intermolecular interactions are affecting intramolecular modes. Indeed, a careful analysis of the 1300–1650 cm^{-1} spectral region reveals small but significant frequency differences between the four polymorphs, as also evidenced by previous works based on the IR studies.[46]

3.2 Surface-Mediated Polymorphs

The mechanisms through which the substrate directs the heterogeneous nucleation of a given phase and the role played in the process by kinetics factors are far from being well understood.[71–74] Generally, phase boundaries produce a lowering in the free energy needed for nucleation. The surface of engineered substrates may act as a template in molecular deposition[75] and the subtle interplay of interactions at the interface may result into altogether new molecular arrangements, which are not observed in the bulk.[76–79] When the interface has the effect of stabilizing forms that would otherwise be metastable under the adopted experimental conditions, the definition "surface stabilized" appears adequate.[80,81] Finally, some thin film phases can be better described as structures which are in fact still related to a parent bulk structure, but perturbed with respect to this as a result of the substrate influence on the growth of the first monolayers.[82–84]

In the following we will describe two instances in which the presence of the surface governs polymorphism in the organic pigments under study. The first instance concerns the case of a surface stabilized polymorph. The thioindigo α polymorph, previously obtained only at high temperatures, can be selectively grown in the bulk form on glass or Si/SiO_2 surfaces. The second instance is the case of a new metastable bulk polymorph of Tyrian purple, whose structure appears to be strictly related to the thin film structures of this dye.

3.2.1 Surface-Stabilized Structure: The α Phase of Thioindigo

The synthetic indigo derivative thioindigo (2-(3-oxo-1-benzothiophen-2(3H)-ylidene)-1-benzothiophen-3(2H)-one) has been known for a long time to display two polymorphs.[51,85] The structures are monoclinic $P2_1/c$ and $P2_1/n$ for polymorphs α and β, respectively, with the two molecules in the unit cell residing on crystal inversion centres. In polymorph α the molecules are stacked along the *b* axis and by projection they appear lying in parallel rows on the plane ac (see Figure 6a). In polymorph β molecules are stacked along axis *a*. Thus, stacking interactions are in both structures exerted between molecules aligned along the shortest axis, with virtually identical intra-stack distances and relative orientations within the stacks. However, in α-thioindigo the stacks are arranged parallel to each other, whereas in β-thioindigo adjacent stacks are rotated.

Even more pronounced than what happens for indigo, DFT-vdW[69] calculations do not give definitive results about the relative stability of the two thioindigo polymorphs, as their energy difference at 0 K is in favour of the β-form but below (≈0.02 kcal/mol) the accuracy threshold of these computational approaches.[86] On the other hand, also the experimental slightly greater density of β at RT points to its thermodynamic stability.[58]

Vapor crystal growth methods always yield the β modification[51,69] unless the temperature is set above 300 °C, in which case the concomitant appearance of both forms is observed, with β-thioindigo still predominant. Solutions drop cast on glass also result in a mixture of the two phases, whereas the same technique never produces pure samples of polymorph β, regardless of the solvent used. However, polymorph α can be obtained as a pure phase from deposition on glass of a xylene solution at 60 °C.

The lattice phonon Raman spectra collected in the investigation of α and β thioindigo polymorphs, establishing the reference spectra for each phase, are shown in Figure 5b along with those simulated with a DFT-vdW method at the experimental room temperature structural parameters.

Both experimental and DFT – vdW simulated spectra of the α (Figure 6b) and β (Figure 6c) polymorphs highlight the distinct lattice mode patterns of the two modifications, which allow for their easy spectroscopic differentiation. The assignments can be carried out in the rigid body approximation framework: for both centrosymmetric monoclinic structures, six Raman-active pure librations of symmetry $3A_g + 3B_g$ should be observed, with virtually no contribution from intramolecular vibrations. These correspond to the peaks below 80 cm^{-1}. Above 100 cm^{-1} the weaker bands detected are nicely simulated in the calculations, which assign them to intramolecular modes whose energies change very little with the structure, as expected for packing polymorphs.

The image of the α-thioindigo single crystals grown by drop cast from xylene are shown on top of the spectra on the right-hand side of Figure 6b. The difference in the intensity of the Raman bands measured on two different orientations of the crystal originates from the crystal strongly anisotropic behavior. The size and the quality of specimens obtained is such that they could be singled out and removed for a single crystal X-ray characterization.

The microRaman measurements suggest that α-thioindigo occurs less frequently in most experimental conditions of growth but can become the only modification appearing on surfaces. The way this knowledge has been exploited to finally fabricate homogeneous films of this form by a shearing method will be presented in Section 4.2.

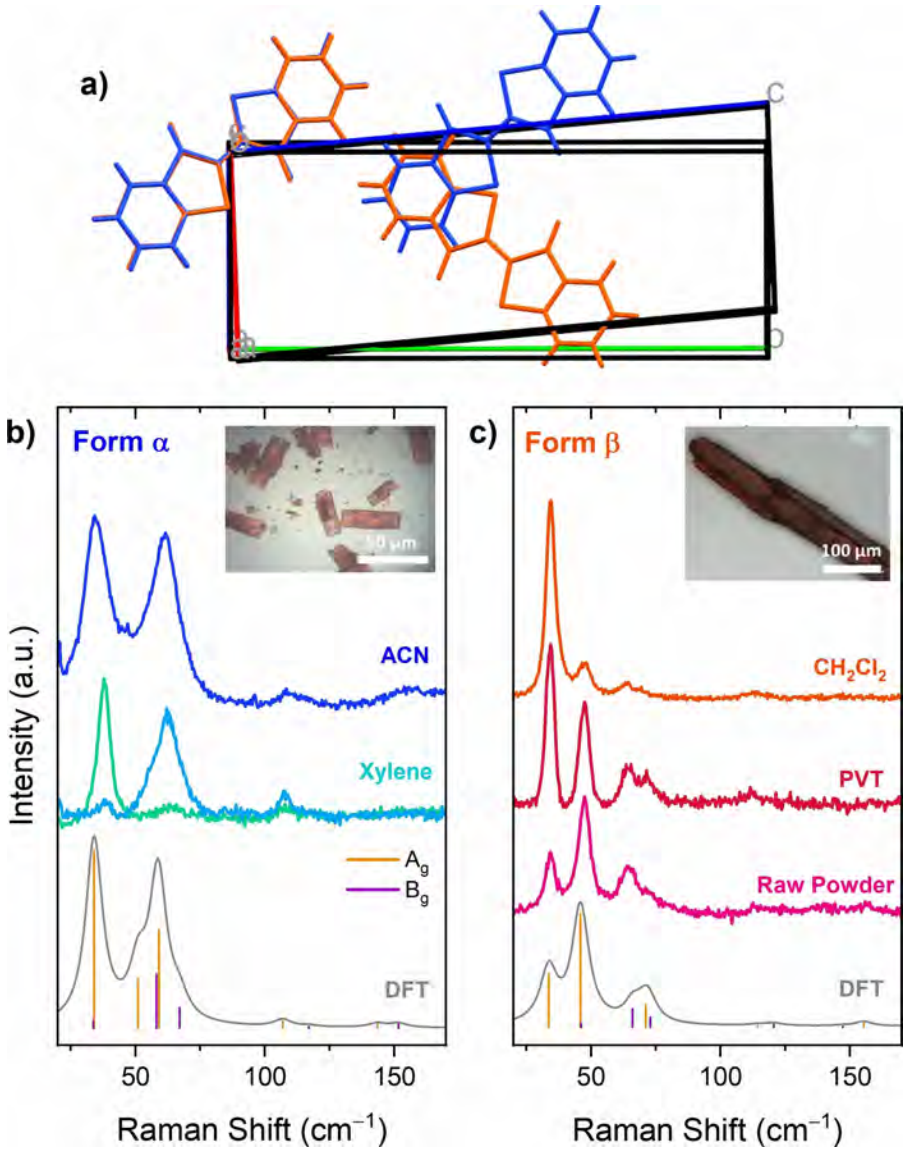

Figure 6. a) Overlay of the packing of the α- and β-thioindigo polymorphs; b) Experimental and unpolarized (powder) simulated DFT-vdW Raman spectra of α-(left) and β-thioindigo (right) crystal samples (see images in the inlets; α crystal obtained from xylene and β from CH_2Cl_2) in the range 10–200 cm^{-1}. Vertical bars of height proportional to the intensity of the mode identify the calculated values, with colour codes yellow and violet for modes of symmetry A_g and B_g, as indicated.

3.2.2 Surface-Induced Structure: The Case of Tyrian Purple

The main component of ancient pigment Tyrian purple is the indigoid of natural origin 6,6-dibromoindigo (Scheme 1), which has in the past years garnered a renewed interest for its ambipolar semiconducting properties in thin-film OFETs.[23,25] The Raman investigation was stimulated by the report of the existence for this system of genuine surface induced or thin film phases, all very similar to each other, identified on several substrates,[87,88] and very different from the single packing configuration so far reported in the literature. In this respect, Tyrian purple constitutes an interesting case among indigoids, because, unlike the previously discussed indigo and thioindigo, the effect of the surface appears to give rise to structures that otherwise would not exist.

Tyrian Form I has a monoclinic $P2_1/c$ structure with two molecules per unit cell (Figure 7a).[79,87,88] The thin-film cell obtained by combining grazing incidence X-ray diffraction data of films deposited on Si/SiO_2 and molecular dynamics simulations for crystal structure prediction[87,88] is instead triclinic $P\bar{1}$ with one molecule per cell on an inversion centre. In both cases intermolecular hydrogen bonds and $\pi-\pi$ stacking interactions are the driving forces for the molecular packing, but only Form I displays a strong similarity with indigo polymorphs.

Israel Journal of Chemistry

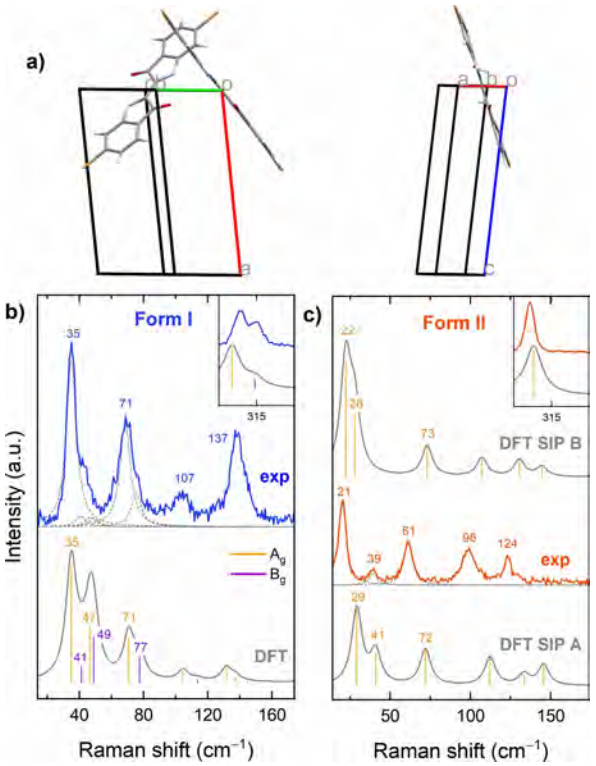

Figure 7. a) Crystal structures of Form I (left) and Form II (right) of tyrian purple; b,c) Experimental and DFT-vdW simulated Raman spectra of Form I and II in the range 10–170 cm^{-1}. Vertical bars of height proportional to the intensity of the mode identify the calculated values, with colour codes yellow and violet for modes of symmetry A_g and B_g, as indicated. Insets: experiments and calculations for the doublet at 309/315 cm^{-1} of Form I and the corresponding single band of Form II. Such a difference can be taken as diagnostic of the different number of molecules per unit cell in their structures.

The low-wavenumber Raman spectrum of a single crystal of Form I obtained by the physical vapor transport method reported in Figure 7 allows for the detection of the lattice phonon vibrations, *i.e.* the fingerprint of the crystal structure.

The vibrational analysis carried out with the help of DFT-vdW simulations and polarized Raman measurements displays in the interval below 100 cm^{-1} the expected six Raman active lattice phonon modes ($3A_g+3B_g$) of the monoclinic structure, which uniquely identifies this polymorph and correspond to pure rotations of the whole molecule. In the range shown in the Figure 7b also some very strong bands assigned to intramolecular modes are recorded (103 and 137 cm^{-1}). Such a feature resembles that of the parent molecule indigo, where the modes of high intensity in the molecular fingerprint region of the spectrum are sensitive to the details of the hydrogen synthons of the crystal structure and can be used for polymorph screening.[57]

The Raman investigation over the low-wavenumber region both of Tyrian commercial powder and sublimed samples identified spectral features such as new bands, broadenings and shifts that could not be related to 6,6-dibromoindigo Form I and suggested the occurrence of a new modification in these specimens. The Raman finding was confirmed by X-ray diffraction analysis of a sublimed polycrystalline sample, which provided a $P\bar{1}$ structure with one molecule per unit cell for a 6,6-dibromoindigo Form II. Notably, the Rietveld refinement of this structure was made possible using the thin-film structures from the literature[88] as a starting input. Finally, the crystalline deposit obtained by drop casting a hot dimethyl sulfoxide solution of the compound on a glass substrate was found to contain two different morphologies (needles and platelets), appearing differently coloured under the polarized light of the microscope. The X-ray measurements of the deposit yielded, besides 6,6-dibromoindigo Form I, a pattern compatible with the presence of Form II lying with the *ab* face on the surface. Once analysed by microRaman, the needles display the low wavenumber Raman spectrum reported in Figure 7b, in which three lattice phonon bands are detected at 21, 39, and 61 cm^{-1}, while two more at 98 and 124 cm^{-1} pertain to intramolecular vibrations. Note that in the framework of the rigid body approximation, only 3 Raman modes of A_g symmetry are predicted to have predominant character of lattice phonons.

A comparison between Form I and Form II spectra in the molecular vibration range is exemplary on how one can draw useful information on structural characteristics also from the analysis of selected intramolecular modes. In the limiting case of a negligible coupling, each molecule in the crystal can be vibrationally excited independently of every other molecule. However, despite being small, the effect of the intermolecular coupling of the internal modes can be still detected for a few low frequency vibrations, as the band of the isolated molecule undergoes a splitting in the crystal. In the Raman spectrum of the centrosymmetric monoclinic structure of Form I this results in doublets, like those reported in the inset of Figure 7b at 309/315 cm^{-1}, whose key feature is that the two components have different polarization properties. The presence of just one band in the same interval for Form II (inset of Figure 7c) confirms that this structure possesses only one molecule per unit cell.

Calculated Raman spectra for Form II and thin film structures are compared to the experiments on Form II crystallites in Figure 7. The calculations clearly highlight strong similarities among all the patterns. Here less than perfect matches should not surprise because even in the presence of structural similarities the spectral features can differ greatly (*e.g.* the indigo polymorphs). Hence, the relevant piece of information conveyed by the spectroscopic data is that the origin of the phases detected in thin films as reported in refs[87,88] can be tracked down to bulk Form II, to which they appear to be closely structurally related.

4. Thin Film Preparation and Characterization

The Raman characterization performed on bulk samples of the pigments under study, which associates a spectroscopic fingerprint to each of the polymorphs, constitutes the prerequisite for the investigation of the phases appearing in films, which is the focus of this Section.

Given the important role played by the interface in phase formation, due to the correlation between molecular packing and charge transport properties in organics,[89–92] the study of growth processes of highly ordered films for device application is the subject of ongoing research.[93–96] In this, the knowledge of the film characteristics benefits from the use of a variety of techniques and Raman is undoubtedly one such tool.

In the manufacture of films, the pigments have the disadvantage of poor solubility, which makes it difficult to prepare them by means of the wet methods preferred by large scale applications, and more expensive and time-consuming dry deposition processes must be used. In the following, we report on the contribution given by Raman to the understanding of the structural properties of indigo thin films grown by high vacuum deposition methods. In addition, we describe how this technique has proved invaluable in addressing the analysis of films of thioindigo and quinacridone obtained with a wet deposition method that circumvented the disadvantage of insolubility. In the case of thioindigo the dye was processed as such, whereas for quinacridone the fabrication involved the deposition of its latent pigment,[97] and the parent system was subsequently recovered via a thermal process.

4.1 Indigo High-Vacuum Evaporated Films and their Phase Composition Question

In Section 3.1.1 it has been shown that the structurally similar A and B indigo polymorphs grow as concomitant in most experimental conditions[57] and it could be assumed that the same was true in the film growths. This information is especially important due to the detrimental effect of a phase mixing on the charge transport.[90,92,98,99]

Specular X-ray scattering measurements of nanometric indigo films vapor deposited on Si/SiO_2[50] yielded only two reflections, which could be assigned to weak crystallographic orientations along different planes of either form A or B,[50] thus not providing a clear indication on the phase composition. Similarly, vapor films grown on various substrates[100] displayed a sharp single diffraction peak, which was taken as an indication of a crystalline texture with a preferential orientation, without however reporting to which polymorph it should be attributed. The issue has been clarified with the help of low-wavenumber Raman spectroscopy in a recent work[101] which provides new insight on the molecular arrangement of indigo on the substrate via the employment of a combination of techniques, confirming the key role of the extended network of intermolecular H-bonds in the growth of these systems.

Figure 8 displays the AFM morphologies of three indigo films deposited in ultra-high vacuum conditions on Si/SiO_2 at different evaporation rates (10, 70 and 200 ng/min), alongside with their specular X-ray and Raman spectra. Independently of the deposition rate, the film thickness is found to be about 40 nm for 1000 ng of deposited molecules. AFM topographies from Figure 8 show that from the lowest (10 ng/min, Figure 8a) to the highest (200 ng/min, Figure 8c) deposition rate, the films consist of 3D grains that evolve progressively from large faced to spherical structures. The morphological evolution of the films is associated with surface smoothening and coverage increase.

The films obtained at 70 and 10 ng/min display identical X-ray diffraction patterns, with only one peak at 10.7°(FWHM = 0.42°) belonging to indigo and corresponding to a d-spacing of 8.28 Å (Figure 8d). No signal for indigo is observed in the film with deposition rate of 200 ng/min.

Observing a single peak in the X-ray diffraction measurement does not clearly allow to diagnose which phase is present, and the situation is similar to that encountered in the literature.[49,50] However, the Raman analysis of the films can rely on the study of the indigo single crystals (Section 3.1.1), which proves that polymorphs A and B can be each identified by their unique spectra. The low-wavenumber spectra of the films in Figure 8e are characterized by three broad bands centred around 41, 92 and 102 cm^{-1}. By deconvolution the pattern can be resolved into the six lattice modes at 40, 42, 74, 84, 92 and 102 cm^{-1} typical of polymorph B, with bandwidths larger than those observed for single crystals (7.5 vs 5.0 cm^{-1}), due to the polycrystalline nature of these samples. The assignment is confirmed by the band splittings at 132/139 cm^{-1} and 1576/1587 cm^{-1} (Figure 8f), already identified as the molecular modes lying at different wavenumbers in the two polymorphs.

Combining the XRD information with the polymorph recognition by Raman spectroscopy, it is thus possible to state that the films are composed only of polymorph B and identify an orientation alongside its (100) plane. The X-ray measurements appear to be missing the crystallinity of the film with the smallest grains, which is instead captured by microRaman. This is probably due the nature of the microscopic technique, which probes ensembles of crystalline domains at a micrometric scale without averaging.

4.2 Solution Shearing of a Pristine Dye: Exploiting the Surface Selectivity of Thioindigo

The limited solubility of thioindigo can be partly overcome by operating at high temperature with suitable solvents. Drop-casting of thioindigo solutions results in scarcely homogeneous films in which often both its polymorphic modifications are present, but the selectivity displayed by the surface for the growth of polymorph α can be exploited to obtain physically pure films of this form, avoiding phase mixing.

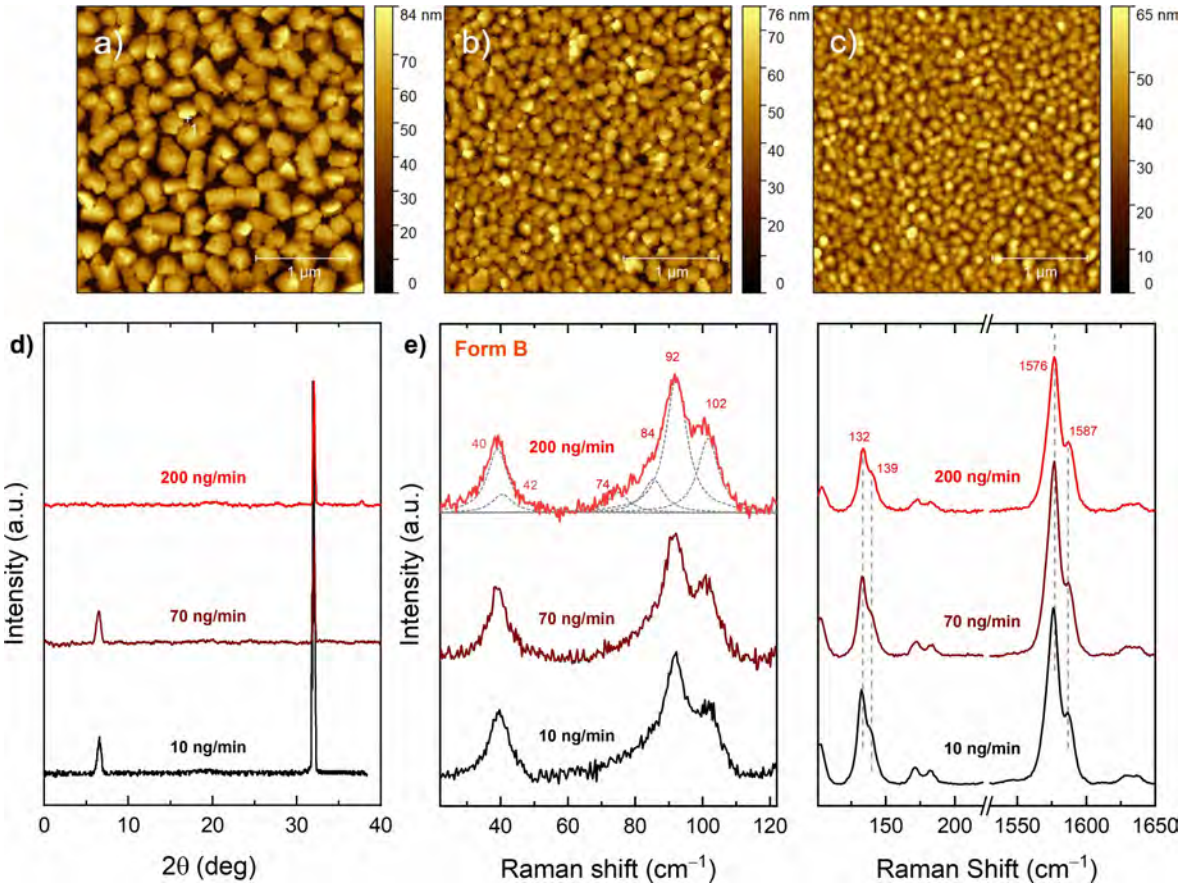

Figure 8. Topographic images of indigo thin films deposited on Si/SiO_2 wafer at room temperature for 10 (a), 70 (b), and 200 ng/min (c) deposition rates. For the same films: XRD patterns (d) and Raman spectra in the energy intervals of lattice phonons (e) and selected internal molecular vibrations (f). The lattice phonon Raman spectrum of the 200 ng/min sample has been deconvoluted to allow the comparison with the spectrum of indigo polymorph B.

The bar-assisted meniscus shearing (BAMS) growth method is the effective technique which has allowed the morphology and polymorphism in thioindigo films to be controlled.[90,91,102,103] Figure 9a reports the scheme of the BAMS setup used for the preparation of the films. The compound solution, forming a meniscus between a metallic bar and the substrate, is dragged along the heated interface at a controlled speed, while the solvent evaporates giving rise to a homogenous deposition.

The optical image of the film collected in cross-polarization of Figure 9b suggests the presence of a texture because of the macroscopic alignment of the domains along the shearing direction.

Low-wavenumber Raman was used to probe the film polymorphic composition and texture by means of experiments in polarized light. This was made by orienting the film either along or perpendicular to the shearing direction, and in turn adjusting the polarizations of the exciting and scattered electric fields of the radiation also parallel or perpendicular to it (Figure 9c). After allowing for some band broadening, it tuns out that the polarized Raman spectra nearly coincide with the patterns collected from the *ab* face of the α-thioindigo single crystal. This substantiates the idea that the film is made up of a collection of domains in which face *ac* lies on the substrate while axis *a* is statistically aligned in the spreading direction. To take care of an angular spread in the ab plane alignment, experimental Raman spectra were fitted to the overlap of a collection of DFT-vdW spectra of the single crystal *ab* face Gaussian distributed about such a direction. The result of the best agreement with the experiments is shown in the Figure, and corresponds to an average spread of 21°, a finding which matches also the results of rotating grazing incidence X-ray diffraction (GIXD) measurements, whose details are given in Rivalta et al.[69]

4.3 The Latent Pigment Method at Work in Film Deposition

The latent pigment method was developed by Zambounis et al. on pyrrolopyrrole pigments to overcome the problem of the low solubility of these systems[104] and first applied to quinacridone (QA) by Imura et al.[97] Quinacridone latent

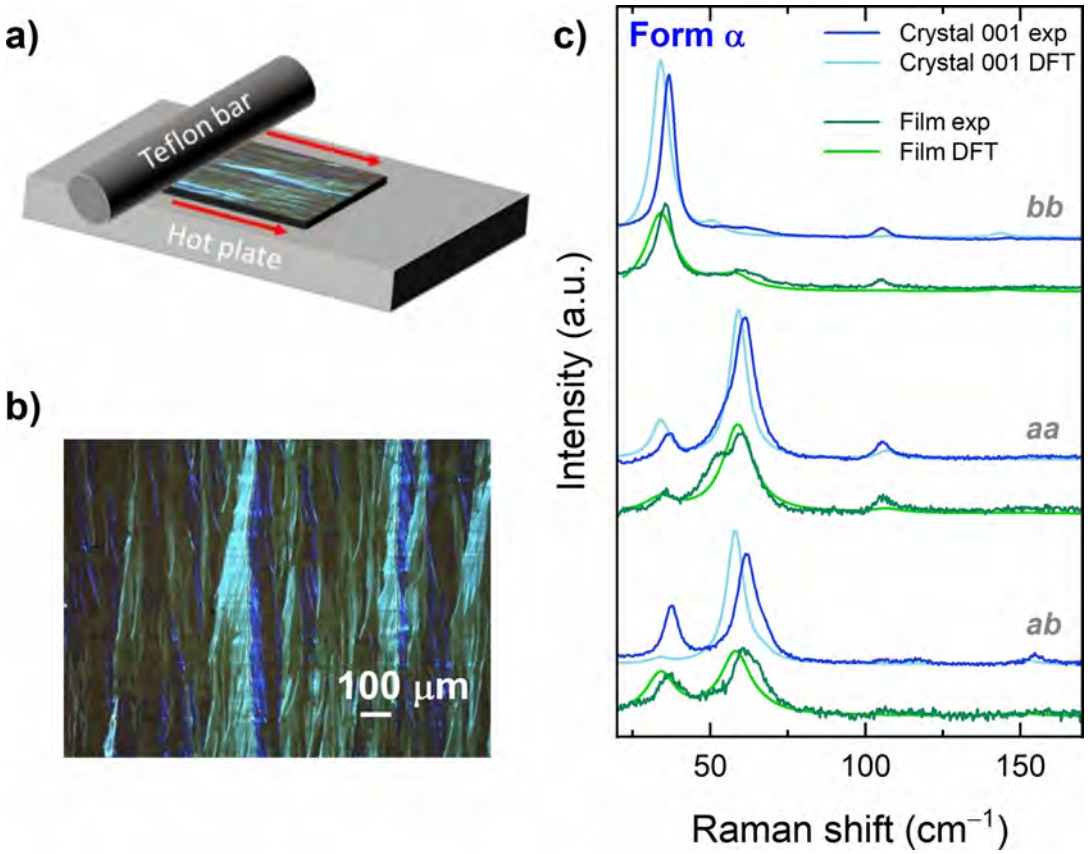

Figure 9. a) Scheme of the BAMS apparatus; b) optical image in cross polarization of α-thioindigo thin film obtained by BAMS from anisole solution; c) polarized lattice phonon Raman spectra of the film oriented along the shearing direction. The spectra are compared to those recorded on the (100) face of a single crystal of α-thioindigo, to the DFT-vdW simulations for the same face and to those resulting from the fit of a Gaussian distribution of crystal orientations about the shearing direction.

pigment (^{t}Boc-QA) is a bright yellow soluble compound prepared by functionalizing the NH functionality of the dye with the ^{t}Boc (tert-butyloxycarbonyl) group, whose role is the transient disruption of the intermolecular hydrogen bonds which cause the low solubility. The latent pigment can be easily deposited by wet methods, while the parent species is subsequently recovered by the thermochemical cleavage of the ^{t}Boc groups as reported in scheme 2.

Homogenous thin films of the chemical precursor ^{t}Boc-QA on Si/SiO_2 substrate were prepared both by spin-coating and BAMS deposition techniques, and the complete thermal removal of the ^{t}Boc group could be assessed both visually by a change of colour and by XRD and spectroscopic measurements.[105–107]

FTIR spectroscopy is a well-established method to verify that the process of deprotection has been brought to completion, by probing the appearance of the N–H stretching band between 3000 cm^{-1} and 3200 cm^{-1} and the intensity weakening of the C=O stretching.[105] Raman microscopy is complementary to FTIR in checking the removal of the ^{t}Boc groups in the range of the intramolecular vibrations, while providing information in the lattice phonon region on the crystal state of the film at all stages of the process.

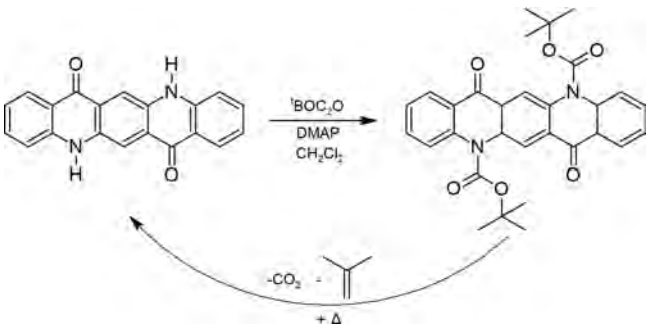

Scheme 2. Synthetic route from quinacridone pigment (QA) to the latent pigment (^{t}Boc-QA) and its thermochemical recovering process.

Figure 10 reports the Raman spectra of the ^{t}Boc-QA spin-coated and BAMS films before and after the deprotection process in all the wavenumber intervals of interest, together with their optical images acquired in cross-polarization.

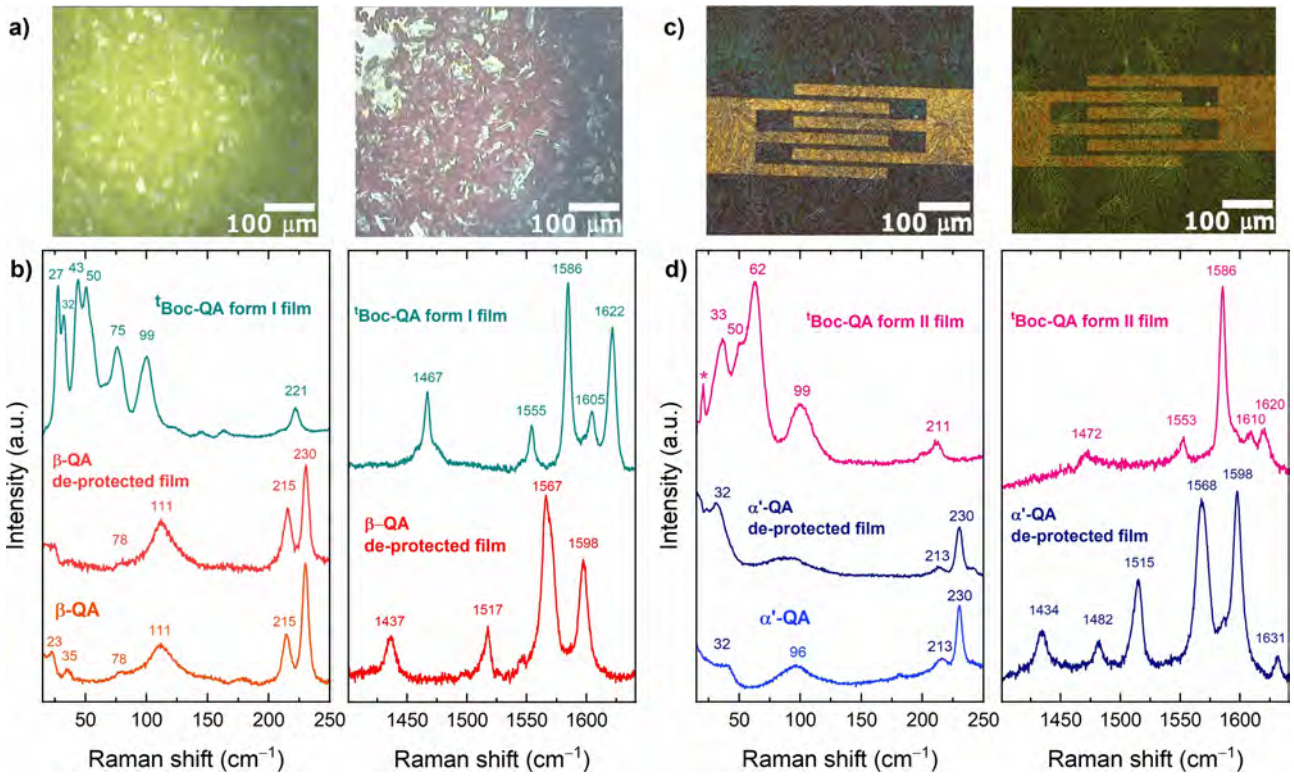

Figure 10. Optical images (a) and Raman spectra (b) of spin-coated ^{t}Boc-QA films before and after thermal deprotection; optical images (c) and Raman spectra (d) of BAMS ^{t}Boc-QA films before and after thermal deprotection. The spectra are compared to α^{I}-QA and β-QA literature data[45] both in the lattice phonon range and in the diagnostic 1400–1700 cm^{-1} interval of intramolecular vibrations.

As can be seen from the images, the crystalline structure of the deposited film is maintained after heating. This suggests that the solid-state chemical reaction is crystal-to-crystal in nature, meaning that the disrupted lattice of the reactant ^{t}Boc-QA rearranges itself to form that of the final product. The selected 1400–1800 cm^{-1} range of intramolecular vibrations (Figure 10d and 10 h for spin coated and BAMS samples, respectively) contains the bands related to the ^{t}Boc cleavage process. In particular, the strong bands at 1567 and 1598 cm^{-1} appearing in the film after deprotection are associated to the QA in-plane total symmetric NRH bending modes and are thus missing in the latent pigment spectrum. It is worth mentioning that despite clearly originating from the same chemical species, the spectra of the precursor in the films prepared with different techniques differ in position and relative intensities of the bands.

The analysis of the low-wavenumber region of the regenerated QA spin-coated films revealed the presence of the QA β-polymorph, whose spectrum in a powder form is given for comparison in Figure 10c. The recognizable features are those below 50 cm^{-1} in addition to the bands at 111 cm^{-1} and at 78 cm^{-1}. This finding agrees with the first reports of bulk QA and QA films prepared by the latent pigment method.[97,106]

After deprotection, the films prepared by BAMS turned out instead to be entirely composed of the metastable α^{I}-QA polymorph. Also in this case the polymorph recognition can be done by comparison of the Raman lattice phonon spectrum of the film with that of the α^{I}-QA single crystal (see Section 3.1.2).[45,107] The assignment is unambiguous, due to the presence of the characteristic structureless band of the triclinic form with a maximum at 97 cm^{-1}.

Since the films were fabricated on identical substrates and underwent similar regeneration processes, the reason of the different growth must be sought in the crystal nature of the precursor in the two cases. Indeed, the lattice phonon spectrum of the ^{t}Boc-QA samples prepared by spin coating (Figure 10c) corresponds to that found for the only crystal structure given in the literature for this compound, and commonly obtained after its synthesis.[108] The occurrence of an altogether different lattice phonon spectrum in the ^{t}Boc-QA BAMS films (Figure 10g) can be ascribed to the presence of a second new polymorphic modification (Form II), whose growth is presumably induced either by the higher temperature employed in the deposition method or by shearing crystallisation process. A discussion of the structural differences between ^{t}Boc-QA Forms I and II is given in reference.[107]

The metastable α^{I}-QA polymorph is thus obtained during the post deposition processing by the polymorphism of its chemical precursor, which depends on its preparation method. The novelty to highlight here is that the identification of the new crystal Form II was made possible by the detection of its unique pattern in the Raman spectrum of the lattice vibrations.

In retrospect, its occurrence also justifies the differences observed in the spectrum of intramolecular vibrations of the films deposited with the different methods. These in fact can be attributed to the different geometries of the ^{t}Boc-QA molecule in the two polymorphs, to the different number of molecules in their unit cells and to their different molecular orientations with respect to the substrate.

5. Summary

This Review has covered the subject of the structural characterization by Raman spectroscopy of organic dyes with semiconducting behavior, the ongoing investigations of which is inspired by their potential eco- and bio-compatibility. The solid state of these systems is marked by widespread polymorphism, as expected for molecular materials. In some of them, such as indigo, the phenomenon manifests itself in slightly dissimilar structures; in others, such as quinacridone, the interplay between the different types of forces produces the appearance of many different structures. In all cases the skill of accessing and identifying the polymorphs constitutes the prerequisite for the full exploitation of the charge transport properties of the semiconductor, which lies in the understanding of the relationship between its electronic and crystalline structures.

We believe that in this, albeit necessarily limited, collection of examples, we have succeeded in demonstrating that non-destructive, non-invasive Raman spectroscopy, especially when employed in the low-wavenumber range, has lent itself effectively to the polymorph characterization of the systems. Working in synergy with X-ray diffraction or electron microscopy, which are the techniques needed for structural determination, Raman can thus complement and complete these sources of information. Bulk single crystals, polycrystalline samples and thin films can be dealt with by THz Raman. Polarization dependent measurements allow accessing the polarization dependent activity of Raman bands and this can be exploited to gain insight on crystal and molecular orientations in the film, also in cases that represent a challenge for other techniques.

Future challenges lie in the use of the low-wavenumber Raman spectroscopy for the study of the structural dynamics and of the anharmonicity which are the main factors governing the charge carrier mobility in semiconductors giving insights on the charge transport mechanism.

Acknowledgements

This work has been funded by the PRIN project “From natural to artificial light-harvesting systems: unveiling fundamental processes toward a bio-inspired materials design” (HARVEST) protocol 201795SBA3. The authors acknowledge Prof. Raffaele Guido Della Valle (University of Bologna), Dr. Arianna Rivalta (University of Bologna), Dr. Simone D’Agostino (University of Bologna) and Dr. Cristiano Albonetti (ISMN-CNR) for the help with DFT-vdW calculations, data elaboration, X-ray diffraction and AFM measurements, respectively. TS thanks Dr. Omer Yaffe (Weizmann Institute of Science) for fruitful discussions. We thank CINECA Supercomputing Center for providing computer time through the ISCRA scheme (project C-SCSCDFT). Open Access Funding provided by Universita di Bologna within the CRUI-CARE Agreement.

References

[1] H. Akamatu, H. Inokuchi, *J. Chem. Phys.* **1950**, *18*, 810–811.
[2] H. Mette, H. Pick, *Z. Phys.* **1953**, *134*, 566–575.
[3] R. A. Nawrocki, N. Matsuhisa, T. Yokota, T. Someya, *Adv. Electron. Mater.* **2016**, *2*, 2–5.
[4] M. Kaltenbrunner, T. Sekitani, J. Reeder, T. Yokota, K. Kuribara, T. Tokuhara, M. Drack, R. Schwödiauer, I. Graz, S. Bauer-Gogonea, S. Bauer, T. Someya, *Nature* **2013**, *499*, 458–463.
[5] D. Natali, *Org. Flex. Electron.* **2021**, 1–25.
[6] H. Zhu, E. S. Shin, A. Liu, D. Ji, Y. Xu, Y. Y. Noh, *Adv. Funct. Mater.* **2020**, *30*, 1–36.
[7] C. Sun, X. Wang, M. A. Auwalu, S. Cheng, W. Hu, *EcoMat* **2021**, *3*, 1–22.
[8] E. D. Głowacki, M. Irimia-Vladu, M. Kaltenbrunner, J. Gsiorowski, M. S. White, U. Monkowius, G. Romanazzi, G. P. Suranna, P. Mastrorilli, T. Sekitani, S. Bauer, T. Someya, L. Torsi, N. S. Sariciftci, *Adv. Mater.* **2013**, *25*, 1563–1569.
[9] E. D. Głowacki, G. Voss, N. S. Sariciftci, *Adv. Mater.* **2013**, *25*, 6783–6800.
[10] M. Irimia-Vladu, N. S. Sariciftci, S. Bauer, *J. Mater. Chem.* **2011**, *21*, 1350–1361.
[11] M. Irimia-Vladu, Y. Kanbur, F. Camaioni, M. E. Coppola, C. Yumusak, C. V. Irimia, A. Vlad, A. Operamolla, G. M. Farinola, G. P. Suranna, N. et al. González-Benitez, *Chem. Mater.* **2019**, *31*, 6315–6346.
[12] H. Kim, G. Kim, I. Song, J. Lee, H. Abdullah, C. Yang, J. H. Oh, *RSC Adv.* **2018**, *8*, 14747–14752.
[13] G. Lanzani, *Nat. Mater.* **2014**, *13*, 775–776.
[14] T. Someya, S. Bauer, M. Kaltenbrunner, *MRS Bull.* **2017**, *42*, 124–130.
[15] P. G. Karamertzanis, G. M. Day, G. W. A. Welch, J. Kendrick, F. J. J. Leusen, M. A. Neumann, S. L. Price, *J. Chem. Phys.* **2008**, *128*, DOI 10.1063/1.2937446.
[16] J. Bernstein, *Polymorphism in Molecular Crystals*, Oxford Science Publications, Oxford, **2002**.
[17] D. Gentili, M. Gazzano, M. Melucci, D. Jones, M. Cavallini, *Chem. Soc. Rev.* **2019**, *48*, 2502–2517.
[18] D. R. Maslennikov, A. Y. Sosorev, R. S. Fedorenko, Y. N. Luponosov, S. A. Ponomarenko, V. V. Bruevich, *J. Phys. Chem. C* **2019**, *123*, 27242–27250.
[19] A. Brillante, I. Bilotti, R. G. Della Valle, E. Venuti, M. Masino, A. Girlando, *Adv. Mater.* **2005**, *17*, 2549–2553.
[20] A. Brillante, I. Bilotti, R. G. Della Valle, E. Venuti, A. Girlando, *CrystEngComm* **2008**, *10*, 937–946.
[21] S. Wood, J. R. Hollis, J. S. Kim, *J. Phys. D* **2017**, *50*, 73001.
[22] I. Y. Chernyshov, M. V. Vener, E. V. Feldman, D. Y. Paraschuk, A. Y. Sosorev, *J. Phys. Chem. Lett.* **2017**, *8*, 2875–2880.

[23] E. D. Glowacki, L. Leonat, G. Voss, M. Bodea, Z. Bozkurt, M. Irimia-Vladu, S. Bauer, N. S. Sariciftci, *Org. Semicond. Sensors Bioelectron. IV* **2011**, *8118*, 81180 M.
[24] E. D. Gowacki, L. Leonat, G. Voss, M. A. Bodea, Z. Bozkurt, A. M. Ramil, M. Irimia-Vladu, S. Bauer, N. S. Sariciftci, *AIP Adv.* **2011**, *1*, 042132.
[25] E. D. Głowacki, G. Voss, L. Leonat, M. Irimia-Vladu, S. Bauer, N. S. Sariciftci, *Isr. J. Chem.* **2012**, *52*, 540–551.
[26] N. Bedoya-Martínez, B. Schrode, A. O. F. Jones, T. Salzillo, C. Ruzié, N. Demitri, Y. H. Geerts, E. Venuti, R. G. Della Valle, E. Zojer, R. Resel, *J. Phys. Chem. Lett.* **2017**, *8*, 3690–3695.
[27] T. Salzillo, A. Giunchi, M. Masino, N. Bedoya-MartÍnez, R. G. Della Valle, A. Brillante, A. Girlando, E. Venuti, *Cryst. Growth Des.* **2018**, *18*, 4869–4873.
[28] N. Bedoya-Martínez, A. Giunchi, T. Salzillo, E. Venuti, R. G. Della Valle, E. Zojer, *J. Chem. Theory Comput.* **2018**, *14*, 4380–4390.
[29] S. Nikodemski, A. A. Dameron, J. D. Perkins, R. P. O'Hayre, D. S. Ginley, J. J. Berry, *Sci. Rep.* **2016**, *6*, 1–8.
[30] M. Asher, D. Angerer, R. Korobko, Y. Diskin-Posner, D. A. Egger, O. Yaffe, *Adv. Mater.* **2020**, *32*, 1908028.
[31] T. Salzillo, R. G. Della Valle, E. Venuti, A. Brillante, T. Siegrist, M. Masino, F. Mezzadri, A. Girlando, *J. Phys. Chem. C* **2016**, *120*, 1831–1840.
[32] T. Salzillo, R. G. Della Valle, E. Venuti, G. Kociok-Köhn, M. Masino, A. Girlando, A. Brillante, *J. Cryst. Growth* **2019**, *516*, 45–50.
[33] J. Socci, T. Salzillo, R. G. Della Valle, E. Venuti, A. Brillante, *Solid State Sci.* **2017**, *71*, 146–151.
[34] A. L. Glebov, O. Mokhun, A. Rapaport, S. Vergnole, V. Smirnov, L. B. Glebov, *Micro-Optics 2012* **2012**, *8428*, 84280 C.
[35] H. Okajima, H. O. Hamaguchi, *Appl. Spectrosc.* **2009**, *63*, 958–960.
[36] H. Hisada, M. Inoue, T. Koide, J. Carriere, R. Heyler, T. Fukami, *Org. Process Res. Dev.* **2015**, *19*, 1796–1798.
[37] K. Bērziņš, S. J. Fraser-Miller, K. C. Gordon, *Int. J. Pharm.* **2021**, *592*, 120034.
[38] R. J. Davey, *Chem. Commun.* **2003**, *3*, 1463–1467.
[39] W. C. McCrone, in *Phys. Chem. Org. Solid State* (Eds.: D. Fox, M. M. Labes, A. Weissberger), Interscience Publishers, London, **1965**, pp. 725–767.
[40] A. Nangia, *Acc. Chem. Res.* **2008**, *41*, 595–604.
[41] D. E. Braun, T. Gelbrich, V. Kahlenberg, G. Laus, J. Wieser, U. J. Griesser, *New J. Chem.* **2008**, *32*, 1677–1685.
[42] A. J. Cruz-Cabeza, J. Bernstein, *Chem. Rev.* **2014**, *114*, 2170–2191.
[43] T. L. Threlfall, *Analyst* **1995**, *120*, 2435–2460.
[44] M. Irimia-Vladu, Y. Kanbur, F. Camaioni, M. E. Coppola, C. Yumusak, C. V. Irimia, A. Vlad, A. Operamolla, G. M. Farinola, G. P. Suranna, N. González-Benitez, M. C. Molina, L. F. Bautista, H. Langhals, B. Stadlober, E. D. Głowacki, N. S. Sariciftci, *Chem. Mater.* **2019**, *31*, 6315–6346.
[45] T. Salzillo, A. Rivalta, N. Castagnetti, S. D'Agostino, M. Masino, F. Grepioni, E. Venuti, A. Brillante, A. Girlando, *CrystEngComm* **2019**, *21*, 3702–3708.
[46] C. Binant, B. Guineau, A. Lautié, *J. Soc. Dyers Colour.* **1990**, *106*, 187–191.
[47] A. O. F. Jones, B. Chattopadhyay, Y. H. Geerts, R. Resel, *Adv. Funct. Mater.* **2016**, *26*, 2233–2255.
[48] J. C. Splitstoser, T. D. Dillehay, J. Wouters, A. Claro, *Sci. Adv.* **2016**, *2*, 2–5.
[49] D. V. Anokhin, L. I. Leshanskaya, A. A. Piryazev, D. K. Susarova, N. N. Dremova, E. V. Shcheglov, D. A. Ivanov, V. F. Razumov, P. A. Troshin, *Chem. Commun.* **2014**, *50*, 7639–7641.
[50] B. Scherwitzl, R. Resel, A. Winkler, *J. Chem. Phys.* **2014**, *140*, 184705.
[51] H. von Helle, *Bull. Soc. Chim. Fr.* **1955**, 1438.
[52] E. A. Gribova, G. S. Zhdanov, G. A. Golder, *Kristallografiya* **1956**, *1*, 53.
[53] P. Susse, A. Wolf, *Naturwissenschaften* **1980**, *67*, 453.
[54] P. Susse, M. Steins, V. Kupcik, *Zeitschrift für Krist. - New Cryst. Struct.* **1988**, *184*, 269–273.
[55] F. Kettner, L. Hüter, J. Schäfer, K. Röder, U. Purgahn, H. Krautscheid, *Acta Crystallogr. Sect. E* **2011**, *E67*, o2867.
[56] A. Burger, R. Ramberfer, *Mikrochim. Acta* **1979**, *2*, 259–271.
[57] T. Salzillo, S. D'Agostino, A. Rivalta, A. Giunchi, A. Brillante, R. G. Della Valle, N. Bedoya-Martínez, E. Zojer, F. Grepioni, E. Venuti, *J. Phys. Chem. C* **2018**, *122*, 18422–18431.
[58] J. Bernstein, R. J. Davey, J. O. Henck, *Angew. Chem. Int. Ed.* **1999**, *38*, 3440–3461; *Angew. Chem.* **1999**, *111*, 3646–3669.
[59] E. Tatsch, B. Schradert, *J. Raman Spectrosc.* **1995**, *26*, 467–473.
[60] W. Lüttke, H. Hermann, M. Klessinger, *Angew. Chem. Int. Ed. Engl.* **1966**, *5*, 598–598.
[61] J. D. Dunitz, J. Bernstein, *Acc. Chem. Res.* **1995**, *28*, 193–200.
[62] T. Siegrist, C. Besnard, S. Haas, M. Schiltz, P. Pattison, D. Chernyshov, B. Batlogg, C. Kloc, *Adv. Mater.* **2007**, *19*, 2079–2082.
[63] S. Dunst, E. Karner, M. E. Coppola, G. Trimmel, M. Irimia-Vladu, *Monatsh. Chem.* **2017**, *148*, 863–870.
[64] E. F. Paulus, F. J. J. Leusen, M. U. Schmidt, *CrystEngComm* **2007**, *9*, 131–143.
[65] T. E. Gorelik, C. Czech, S. M. Hammer, M. U. Schmidt, *CrystEngComm* **2016**, *18*, 529–535.
[66] G. Lincke, H. U. Finzel, *J. Biol. Chem.* **1996**, *31*, 441–452.
[67] T. Salzillo, A. Girlando, A. Brillante, *J. Phys. Chem. C* **2021**, *125*, 7384–7391.
[68] G. Turrell, *Infrared and Raman Spectra of Crystals*, Academic Press, London and New York, **1972**.
[69] A. Rivalta, A Multi-Methodological Approach for the Study of Polymorphism in Organic Pigments and Pharmaceuticals, University of Bologna, **2020**.
[70] A. Girlando, M. Masino, A. Brillante, T. Toccoli, S. Iannotta, *Crystals* **2016**, *6*, 41.
[71] J. Simbrunner, B. Schrode, S. Hofer, J. Domke, T. Fritz, R. Forker, R. Resel, *J. Phys. Chem. C* **2021**, *125*, 618–626.
[72] K. Motai, T. Narimatsu, C. Chen, Y. Hayamizu, *J. Mater. Chem. C* **2020**, *8*, 8585–8591.
[73] J. Jin, S. Wu, Y. Ma, C. Dong, W. Wang, X. Liu, H. Xu, G. Long, M. Zhang, J. Zhang, W. Huang, *ACS Appl. Mater. Interfaces* **2020**, *12*, 19718–19726.
[74] P. K. Verma, L. Huelsenbeck, A. W. Nichols, T. Islamoglu, H. Heinrich, C. W. Machan, G. Giri, *Chem. Mater.* **2020**, *32*, 10556–10565.
[75] A. Lausi, M. Polentarutti, S. Onesti, J. R. Plaisier, E. Busetto, G. Bais, L. Barba, A. Cassetta, G. Campi, D. Lamba, A. Pifferi, S. C. Mande, D. D. Sarma, S. M. Sharma, G. Paolucci, *Eur. Phys. J. Plus* **2015**, *130*, 43.
[76] A. Rivalta, A. Giunchi, L. Pandolfi, T. Salzillo, S. D'agostino, O. Werzer, B. Schrode, N. Demitri, M. Mas-Torrent, A. Brillante, R. G. Della Valle, E. Venuti, *Dyes Pigm.* **2020**, *172*, 107847.
[77] B. Schrode, A. O. F. Jones, R. Resel, N. Bedoya, R. Schennach, Y. H. Geerts, C. Ruzié, M. Sferrazza, A. Brillante, T. Salzillo, E. Venuti, *ChemPhysChem* **2018**, *19*, 993–1000.

[78] A. Rivalta, T. Salzillo, E. Venuti, R. G. Della Valle, B. Sokolovič, O. Werzer, A. Brillante, *ACS Omega* **2018**, *3*, 9564–9571.
[79] L. Pandolfi, A. Rivalta, T. Salzillo, A. Giunchi, S. D'Agostino, R. G. Della Valle, A. Brillante, E. Venuti, *J. Phys. Chem. C* **2020**, *124*, 17702–17710.
[80] D. Reischl, C. Röthel, P. Christian, E. Roblegg, H. M. A. Ehmann, I. Salzmann, O. Werzer, *Cryst. Growth Des.* **2015**, *15*, 4687–4693.
[81] F. Artusio, R. Pisano, *Int. J. Pharm.* **2018**, *547*, 190–208.
[82] R. Ruiz, D. Choudhary, B. Nickel, T. Toccoli, K. C. Chang, A. C. Mayer, P. Clancy, J. M. Blakely, R. L. Headrick, S. Iannotta, G. G. Malliaras, *Chem. Mater.* **2004**, *16*, 4497–4508.
[83] T. Shirasawa, S. Yanagisawa, S. N. Hatada, W. Voegeli, Y. Morikawa, T. Takahashi, *J. Phys. Chem. C* **2018**, *122*, 6240–6245.
[84] I. Salzmann, D. Nabok, M. Oehzelt, S. Duhm, A. Moser, G. Heimel, P. Puschnig, C. Ambrosch-Draxl, J. P. Rabe, N. Koch, *Cryst. Growth Des.* **2011**, *11*, 600–606.
[85] W. Haase-Wessel, M. Ohmasa, P. Süsse, *Naturwissenschaften* **1977**, *64*, 435.
[86] N. Marom, R. A. Distasio, V. Atalla, S. Levchenko, A. M. Reilly, J. R. Chelikowsky, L. Leiserowitz, A. Tkatchenko, *Angew. Chem. Int. Ed.* **2013**, *52*, 6629–6632; *Angew. Chem.* **2013**, *125*, 6761–6764.
[87] M. Truger, A. O. F. Jones, A. Maria, S. Pachmajer, *J. Cryst. Growth* **2016**, *447*, 73–79.
[88] M. Truger, O. M. Roscioni, C. Rothel, D. Kriegner, C. Simbrunner, R. Ahmed, E. D. Gaowacki, J. Simbrunner, I. Salzmann, A. M. Coclite, A. O. F. Jones, R. Resel, *Cryst. Growth Des.* **2016**, *16*, 3647–3655.
[89] H. Chung, Y. Diao, *J. Mater. Chem. C* **2016**, *4*, 3915–3933.
[90] T. Salzillo, N. Montes, R. Pfattner, M. Mas-Torrent, *J. Mater. Chem. C* **2020**, *8*, 15361–15367.
[91] T. Salzillo, A. Campos, A. Babuji, R. Santiago, S. T. Bromley, C. Ocal, E. Barrena, R. Jouclas, C. Ruzie, G. Schweicher, Y. H. Geerts, M. Mas-Torrent, *Adv. Funct. Mater.* **2020**, *30*, 1–9.
[92] O. D. Jurchescu, D. A. Mourey, S. Subramanian, S. R. Parkin, B. M. Vogel, J. E. Anthony, T. N. Jackson, D. J. Gundlach, *Phys. Rev. B: Condens. Matter Mater. Phys.* **2009**, *80*, 085201.
[93] A. A. Virkar, S. Mannsfeld, Z. Bao, N. Stingelin, *Adv. Mater.* **2010**, *22*, 3857–3875.
[94] H. A. Becerril, M. E. Roberts, Z. Liu, J. Locklin, Z. Bao, *Adv. Mater.* **2008**, *20*, 2588–2594.
[95] D. Liu, Q. Miao, *Mater. Chem. Front.* **2018**, *2*, 11–21.
[96] D. Ho, J. Lee, S. Park, Y. Park, K. Cho, F. Campana, D. Lanari, A. Facchetti, S. Y. Seo, C. Kim, A. Marrocchi, L. Vaccaro, *J. Mater. Chem. C* **2020**, *8*, 5786–5794.
[97] Y. Imura, T. Senju, J. Mizuguchi, *J. Imaging Soc. Japan* **2005**, *44*, 143–147.
[98] A. Tamayo, S. Hofer, T. Salzillo, C. Ruzié, G. Schweicher, R. Resel, M. Mas-Torrent, *J. Mater. Chem. C* **2021**, *9*, 7186–7193.
[99] D. W. Davies, S. K. Park, P. Kafle, H. Chung, D. Yuan, J. W. Strzalka, S. C. B. Mannsfeld, S. G. Wang, Y. S. Chen, D. L. Gray, X. Zhu, Y. Diao, *Chem. Mater.* **2021**, *33*, 2466–2477.
[100] M. Irimia-Vladu, E. D. Gåowacki, P. A. Troshin, G. Schwabegger, L. Leonat, D. K. Susarova, O. Krystal, M. Ullah, Y. Kanbur, M. A. Bodea, V. F. Razumov, H. Sitter, S. Bauer, N. S. Sariciftci, *Adv. Mater.* **2012**, *24*, 375–380.
[101] A. Rivalta, C. Albonetti, D. Biancone, M. Della Ciana, S. d'Agostino, L. Biniek, M. Brinkmann, A. Giunchi, T. Salzillo, A. Brillante, R. G. Della Valle, E. Venuti, *Surfaces and Interfaces* **2021**, *24*, 101058.
[102] T. Salzillo, A. Campos, M. Mas-Torrent, *J. Mater. Chem. C* **2019**, *7*, 10257–10263.
[103] S. Georgakopoulos, F. G. Del Pozo, M. Mas-Torrent, *J. Mater. Chem. C* **2015**, *3*, 12199–12202.
[104] J. S. Zambounis, Z. Hao, A. Iqbal, *Nature* **1997**, *388*, 131–132.
[105] I. Maqueira-Albo, G. Ernesto Bonacchini, G. Dell'Erba, G. Pace, M. Sassi, M. Rooney, R. Resel, L. Beverina, M. Caironi, *J. Mater. Chem. C* **2017**, *5*, 11522–11531.
[106] H. Yanagisawa, J. Mizuguchi, S. Aramakt, Y. Sakat, *Jpn. J. Appl. Phys.* **2008**, *47*, 4728–4731.
[107] L. Pandolfi, A. Giunchi, A. Rivalta, S. D'agostino, R. G. Della Valle, M. Mas-Torrent, M. Lanzi, E. Venuti, T. Salzillo, *J. Mater. Chem. C* **2021**, *Just accep*.
[108] J. Mizuguchi, *Acta Crystallogr. Sect. E* **2003**, *59*, o474–o475.

Manuscript received: July 5, 2021
Revised manuscript received: August 30, 2021
Version of record online: September 15, 2021

